

## **FINITE ELEMENT MODELING OF THE EMBOSSING OF PAPER SHEETS**

**S. Liang and J. C. Suhling,  
Department of Mechanical Engineering  
Auburn University  
Auburn, AL 36849-5341  
U.S.A.**

### **ABSTRACT**

Embossing processes are often used to increase the surface area of low basis weight papers giving them better absorbency properties. They also serve to add surface texture and increase ply bonding in multi-layer papers. The mechanical properties (e.g., stiffness and strength) of paper sheets are significantly effected in a detrimental manner by embossing. In this work, an initial study of the paper embossing process has been performed using finite element analysis. The paper was modeled as a nonlinear inelastic orthotropic solid and the rubber was taken to be an incompressible hyperelastic material. Interface elements were introduced to simulate the behavior of the contact surfaces. Since the measured mechanical properties of the paper under consideration were highly dependent on moisture content, analyses were performed at relative humidity levels of 50% and 90%. Permanent deformations, and residual stresses and strains in embossed paper sheets have been calculated. Also, the changes in the mechanical behavior of paper sheets due to embossing have been predicted.

## INTRODUCTION

Current process and product design needs of the pulp and paper industry provide several challenging problems in engineering mechanics. For example, these materials are often utilized in structural applications such as cones, spiral tubes, and corrugated containers where they are subjected to complicated biaxial and triaxial stress states, including shear. Also, the end utility of many low basis weight paper products (e.g., towel and tissue) is affected significantly by the inherently mechanical processes of creping and embossing. Finally, laminated (multi-ply) papers will curl and develop residual stresses due to environmental changes. At present, lack of reliable modeling methods and accurate mechanical behavior characterization hampers analysis of such problems. Hence, it has been common practice in the paper industry to use trial and error, and empirical approaches for optimizing the designs of manufacturing processes and converted products. Such haphazard approaches will often lead to undesirable product characteristics or unexpected structural failures. Also, the current lack of technology limits creative design improvements which could improve product sales and curtail the excess use of materials and energy. Therefore, more research is needed within the pulp and paper industry to develop fundamental understandings of manufacturing processes and paper material behavior.

A simplified embossing configuration containing a single embossing element is shown in Figure 1. The metal punch (embossing element) is used to permanently deform the paper sheet. The thin paper sheet is laterally pressed by the embossing element into a relatively thick elastic rubber layer of low stiffness. The maximum embossing element penetration depth is chosen to cause inelastic deformation of the paper sheet. After this depth has been reached, the embossing element is retracted, and a non-flat textured sheet remains. Typically, this operation is performed continuously by taking paper off a roll and feeding it between a pair of stainless steel rolls. The first roll is called the embossing roll and contains a pattern of raised embossing elements. The second roll has an outside layer of rubber and is called the backing roll. Embossing processes are designed to increase the surface area of low basis weight papers giving them better absorbency properties. They also serve to add surface texture and increase ply bonding in multi-layer

papers. The mechanical properties (e.g., stiffness and strength) of paper sheets are significantly effected in a detrimental manner by embossing. Thus, the embossing process for towel and tissue represents a tradeoff between increased absorbency and decreased strength and stiffness.

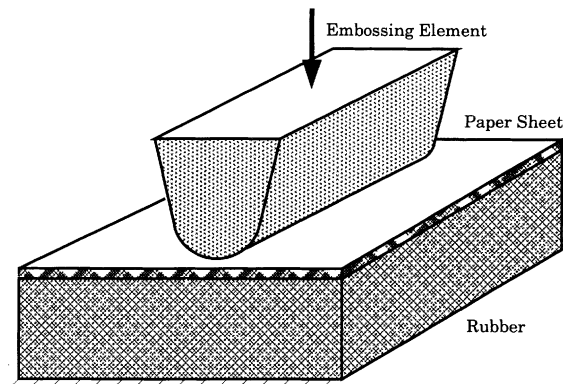


Figure 1 - Simplified Embossing Configuration

The embossing process is a material forming process in which multibody contact is involved. The study of contact problems in elasticity using analytical methods has been reviewed by Lubkin (1). Early finite element models of material contact were presented by Kikuchi (2), and Kikuchi and Oden (3). These authors have also published a detailed monograph on the subject (4). A large volume of work has recently appeared on the study of metal forming problems using finite element methods employing contact with friction. For example, Holzner and Mannl (5), and Sih, et al. (6) have used the finite element method to model elastic-plastic materials with nonlinear hardening which were subjected to axisymmetric sheet metal forming processes. A recent monograph (7) is totally devoted to the use of finite element methods in the modeling of metal forming processes.

In this study, an initial study of the paper embossing process has been performed using finite element analysis. The objective of this investigation was to begin the formulation of a fundamental understanding of the mechanical behavior of paper during a typical embossing process. Several numerical simulations have been performed

using the finite element method. The finite element models included large deformations (geometric nonlinearity), anisotropic nonlinear inelastic material behavior (material nonlinearity), and interface elements to describe contact surfaces (boundary nonlinearity). Advanced computer codes have been used to calculate the permanent deformations, and residual stresses and strains in embossed paper sheets. Both loading and unloading of the material system have been considered. Changes in the stress-strain behavior and material properties of paper sheets due to embossing have been predicted by calculating the uniaxial tension response of the embossed sheets. Extensive experimental material characterization data have been used as input to the finite element models. These data included results of uniaxial, shear, and biaxial testing under different relative humidity levels where the nonlinear and inelastic mechanical behavior of the paper under consideration were measured.

## **FINITE ELEMENT MODELS**

### **General Discussion**

Numerical modeling in this work was performed using an iterative nonlinear finite element approach incorporating nonlinear material behavior and plasticity, large deformations, and contact stresses. All calculations were performed using commercially available computer programs. The finite element software package ABAQUS (Implicit Version) was chosen because of its ability to perform sophisticated nonlinear analyses. It allows for modeling of three-dimensional structures with general user-specified material nonlinearities. Also, it has special functions designed to accommodate large deformations (kinematic nonlinearities) and contact of multiple bodies. All preprocessing (mesh generation and model construction) and postprocessing (data analysis using color graphics) of the finite element models in this work were accomplished using the program PATRAN. The majority of the calculations in this work were performed on Sun SparcStations available on the College of Engineering Computer Network at Auburn University. In addition, ABAQUS calculations were also performed on the Cray X-MP/216 supercomputer operated by the Alabama Supercomputer Network.

## Geometry and Loading

Precise modeling of the embossing of paper sheets is extremely difficult due to the complicated nature of the geometry and nonlinear material behavior, and the existence of material contact. Therefore, in this initial investigation only the idealized single element embossing configuration shown in Figure 1 was considered. In addition, only two-dimensional plane stress and plane strain analyses of this geometry were performed. The analyzed planar configuration is illustrated in Figure 2. Because of symmetry, only the right half of the geometry in Figure 1 was modeled using a finite element mesh since the deformations are symmetric about the center line. The materials from top to bottom are the steel embossing element (considered rigid), paper sheet, and rubber (surface of backing roll). The executed two-dimensional simulations have served as test vehicles on which the performance of the iterative nonlinear finite element models could be evaluated.

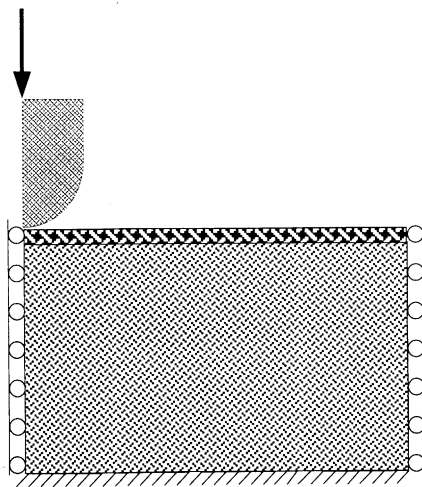


Figure 2 - Planar Embossing Model

As illustrated schematically in Figure 2, the center line of the embossing element was constrained to move vertically. The embossing element was subjected to a prescribed downward displacement, and then this deformation was released. The right edge of the combined material

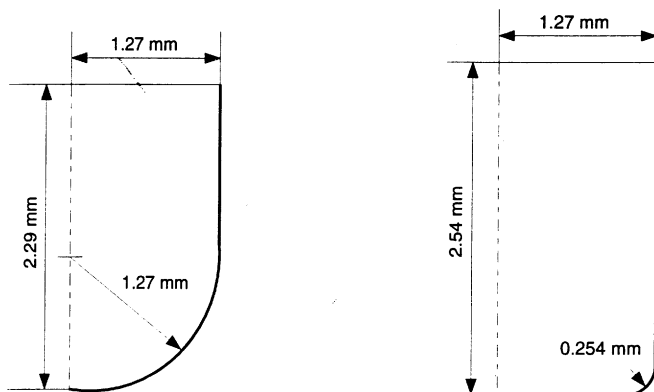
system was constrained to move vertically. Since only the right half of the geometry in Figure 1 was meshed, the centerline of the combined material system was also constrained to move vertically. In the final boundary condition, the bottom edge of the rubber from the backing roll was fully constrained. This condition was chosen since the steel core of the backing roll was considered rigid and perfect bonding was assumed between the rubber and steel.

Finite element meshes for the two-dimensional embossing models were generated using the previously mentioned PATRAN software. The embossing element itself was described using the rigid surface definition procedure available in ABAQUS. Quadrilateral planar elements were then utilized to mesh the paper/rubber material system which is compressed by the embossing element. These elements used linear basis functions with four integration points. Also, elements incorporating general finite deformation formulations were chosen. As discussed in more detail below, the stress-strain relations for the rubber and paper materials were specified using built-in ABAQUS formulations and the results of material characterization experiments.

Two different embossing element cross-sectional shapes were considered in this study. These included a rounded rectangular element and a rounded circular element. Figures 3 and 4 show the chosen cross-sectional dimensions for the two embossing elements, and Figures 5 and 6 show the finite element meshes for the complete two-dimensional embossing models incorporating these elements. In Figures 5 and 6, the top four layers of elements represent the paper material and the bottom 15 layers represent the rubber material. The thickness (vertical dimension) of the paper layer was .254 mm and the thickness of the rubber layer was 2.032 mm. Both layers had a length (horizontal dimension) of 7.620 mm.

The embossing analyses were carried out in three loading steps. In the first step, an embossing element penetration of 1 mm was applied through a prescribed displacement of the embossing element. In the second step, the embossing element was retracted, and the residual stresses and permanent deformations in the paper sheet were calculated. In the final step, the embossing element, rubber layer, and all the interface

elements were removed from the model. Uniaxial tension analyses for loading along the horizontal direction were then performed to monitor the changes in the mechanical response of the paper due to embossing.



Figures 3 and 4 - Embossing Elements

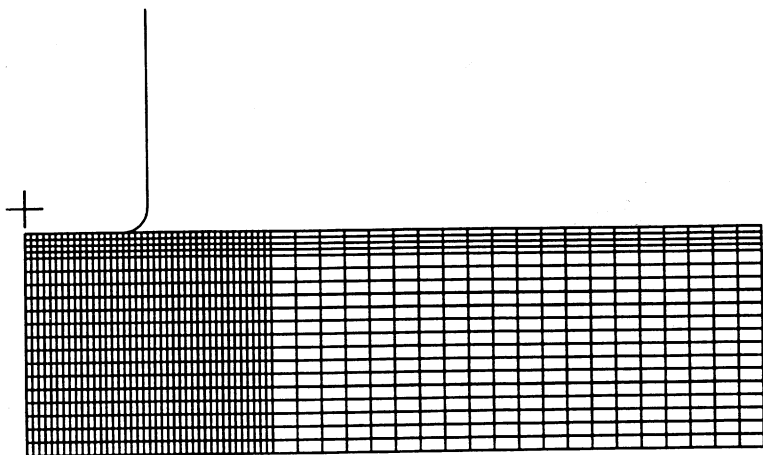


Figure 5 - Finite Element Mesh for Rounded Rectangular Embossing Element

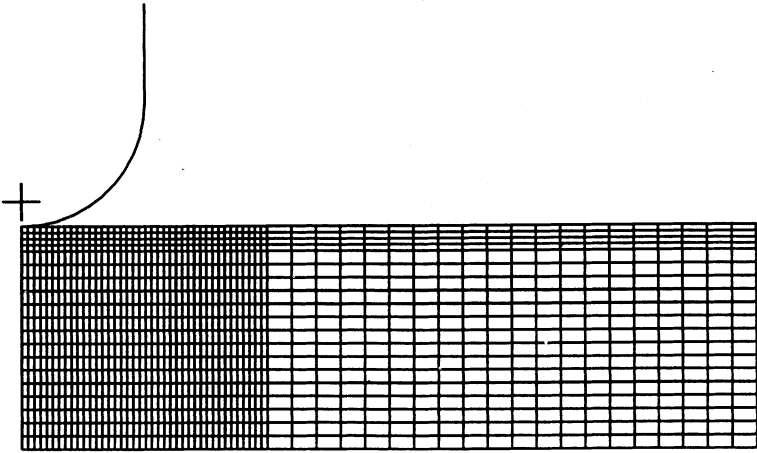


Figure 6 - Finite Element Mesh for Rounded Circular Embossing Element

### Material Contact and Interface Elements

Material contact in the developed finite element models for the embossing process was modeled with the aid of interface elements. These elements were used to connect pairs of points from two materials which contact each other in a manner such that relative sliding can occur. In the embossing simulations, interface finite elements were used between the embossing element and the paper sheet, and also between the paper sheet and the rubber from the backing roll. Type IRS21 rigid surface interface elements were used between the rigid embossing element and the paper sheet. Such interface elements allow sliding over a finite distance along the rigid surface. Between the paper sheet and the rubber layer, type INTER2 interface elements were used to simulate the contact of the two deformable layers. At each integration point of the interface elements, a measure of relative displacement was used to determine whether or not there was contact. In the case of contact, a Lagrange multiplier was introduced at the integration point to impose the constraint that the surfaces cannot interfere. The sign of the Lagrange multiplier was monitored to detect any separation of the surface at that point.

The formulation used for the interface elements in ABAQUS requires them to be characterized by several parameters. These included the initial clearance, the coefficient of friction, the "stiffness of stick", and three so-called interface control parameters. Based on experimental observations, the coefficients of friction were chosen to differ by an order of magnitude:  $\mu = .02$  between the rigid embossing element and the paper sheet, and  $\mu = .2$  between the paper sheet and the rubber layer. The "stiffness of stick" is an elastic stiffness which transmits shear forces across the interface as long as they are below the friction limit. This stiffness is applied using a penalty method procedure. Specification of higher values gives more assurance that no relative motion will occur between contacting surfaces until slip occurs. However, the convergence of the iterative finite element solution procedure will be more rapid when this stiffness is chosen to be smaller. The three interface control parameters allow the user to specify various tolerances which mandate how close various interface conditions are required to be satisfied. In this work, the calculated results from the numerical simulations were found to be very sensitive to the specified values of the "stiffness of stick" and the interface control parameters. It was found that convergence of the iterative finite element simulations to reasonable solutions occurred only when a tedious trial and error process was used to find the optimum values of these parameters.

### Material Behavior - Rubber

In this work, the stress-strain behavior of the rubber was modeled using a hyperelastic (nonlinear elastic) formulation based upon using a strain energy density function. The strain energy density function was chosen so that the hyperelastic model was equivalent to the incompressible two parameter Mooney-Rivlin model for rubber elasticity. The strain energy function for this case is (8,9)

$$U = C_1 (I_1 - 3) + C_2 (I_2 - 3) \quad (1)$$

where  $I_1$  and  $I_2$  are the first and second invariants of a general large deformation strain tensor, and  $C_1$  and  $C_2$  are material constants. Values of  $C_1 = .550$  MPa and  $C_2 = .138$  MPa were chosen based on experimental results for natural rubber. The stress-strain relations can be obtained from the strain energy density function using the general large

deformation constitutive equation for hyperelastic materials (8,10). For the material constants chosen in this work, the constitutive formulation for rubber yielded the uniaxial stress-strain curve illustrated in Figure 7.

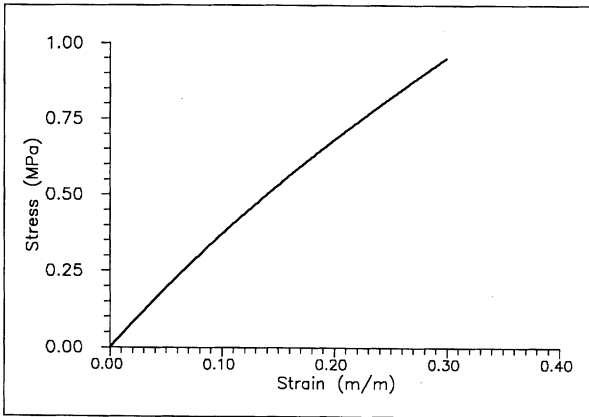


Figure 7 - Rubber Uniaxial Stress-Strain Curve

### Material Behavior - Paper

As surveyed by Perkins (11) and Suhling (12), paper and paperboard have been modeled macroscopically using elastic, viscoelastic, and inelastic formulations. Several continuum theories have been established for a paper sheet or laminate viewed as a three-dimensional orthotropic solid medium. The theory of linear orthotropic elasticity has been most often utilized to model the macroscopic behavior of papers. Since the mechanical behavior of most papers is highly nonlinear even at low strains, a linear elastic approach is especially unsuitable in the analysis of the embossing process, where high strains and permanent (inelastic) deformations take place.

There have been only a limited number of studies which have considered nonlinear elastic models (13-15) for the stress-strain behavior of paper. Even fewer have utilized elastic-plastic constitutive models (16-17). In the work of Ramasubramanian and Ko (16), a nonlinear finite element analysis (using ABAQUS) of the spherical ball penetration test for paper was performed. In their study, an elastic-plastic constitutive model for

paper was incorporated which included strain hardening patterned after measured uniaxial stress-strain data. Perkins, et al. (17) have proposed a new continuum elastic-plastic constitutive model for paper. Their theory is based on applying the minimum deformation work concepts introduced by Tate (18).

In this initial investigation on the embossing of paper, a incremental plasticity model with isotropic hardening (as commonly used for metals) was chosen to model the mechanical behavior of the paper material (8,10). The paper was considered to be orthotropic linear elastic until onset of inelastic behavior. The stress-strain relations before yielding then have the form

$$\begin{aligned} \varepsilon_x &= \frac{1}{E_1} [\sigma_x - \nu_{12}\sigma_y - \nu_{13}\sigma_z] & \gamma_{xz} &= \frac{\tau_{xz}}{G_{13}} \\ \varepsilon_y &= \frac{1}{E_2} [\sigma_y - \nu_{21}\sigma_x - \nu_{23}\sigma_z] & \gamma_{yz} &= \frac{\tau_{yz}}{G_{23}} \\ \varepsilon_z &= \frac{1}{E_3} [\sigma_z - \nu_{31}\sigma_x - \nu_{32}\sigma_y] & \gamma_{xy} &= \frac{\tau_{xy}}{G_{12}} \end{aligned} \quad (2)$$

where  $E_1, E_2, E_3$  are the elastic moduli,  $\nu_{12}, \nu_{21}, \nu_{13}, \nu_{31}, \nu_{23}, \nu_{32}$  are the Poisson's ratios,  $G_{13}, G_{23}, G_{12}$  are the shear moduli, and the  $(x,y,z)$  coordinate system has been aligned with the material symmetry directions of the paper ( $x = MD, y = CD$ ). The Poisson's ratios in eq. (2) are related through the formula

$$\frac{\nu_{ij}}{E_i} = \frac{\nu_{ji}}{E_j} \quad (i, j = 1, 2, 3) \quad (3)$$

Onset of plastic deformation was predicted using the anisotropic failure criterion of Hill (19,20). This criterion is an anisotropic extension of the Von Mises theory for isotropic materials. In terms of the stress components in the  $(x,y,z)$  coordinate system aligned with the directions of material symmetry, this criterion predicts that inelastic behavior initiates when

$$A(\sigma_x - \sigma_y)^2 + B(\sigma_x - \sigma_z)^2 + C(\sigma_y - \sigma_z)^2 + D\tau_{xz}^2 + E\tau_{yx}^2 + F\tau_{xy}^2 = 1 \quad (4)$$

Quantities A, B, C, D, E, F in eq. (4) are material dependent strength parameters evaluated using

$$\begin{aligned} A &= \frac{1}{2} \left[ \frac{1}{X^2} + \frac{1}{Y^2} - \frac{1}{Z^2} \right] & D &= \frac{1}{Q^2} \\ B &= \frac{1}{2} \left[ \frac{1}{X^2} + \frac{1}{Z^2} - \frac{1}{Y^2} \right] & E &= \frac{1}{R^2} \\ C &= \frac{1}{2} \left[ \frac{1}{Y^2} + \frac{1}{Z^2} - \frac{1}{X^2} \right] & F &= \frac{1}{S^2} \end{aligned} \quad (5)$$

where X, Y, Z are the measured uniaxial "yield" stresses in the x, y, z directions, respectively, and Q, R, S are the measured pure shear "yield" stresses.

After the onset of inelastic behavior at a point, plastic material behavior was predicted using an isotropic hardening formulation (8). The hardening curve was obtained from the shape of the x-direction (MD) stress-strain curve after yielding. Reduced material stiffnesses were then obtained from the instantaneous slope of the hardening curve. When unloaded, the stiffnesses were changed back to their elastic (initial) values. Such behavior is common in metals subjected to loading and unloading in uniaxial tension, and is also exhibited by paper.

The main types of paper materials which have been examined in this study have been low basis weight towel and tissue grades. Due to the highly proprietary nature of this ongoing work, results for such papers are not shown in this publication. Rather, the paper material considered herein was a higher basis weight linerboard grade which the authors have studied in other projects. In particular, this work reports results for machine made 100% Lakes States softwood unbleached Kraft paper (basis weight 205 g/m<sup>2</sup>, mass density 670 kg/m<sup>3</sup>). Although the presented results cannot be directly extended to towel and tissue, they serve to illustrate the nature of the method and the potential benefits of the calculations.

Extensive experimental material characterization data have been used as input to the constitutive and failure models for paper discussed above. Since the characteristic mechanical response of paper is highly affected by its moisture content, material property data obtained at two different relative humidity levels were considered. Experimental data were measured in a specially constructed environmental chamber at relative humidity levels of 50% and 90%. Details of the experimental procedure and the obtained results are contained in a separate publication by one of the authors (21). Figures 8 and 9 show uniaxial tensile stress-strain curves obtained in the  $x = \text{MD}$  and  $y = \text{CD}$  testing orientations at relative humidity levels of 50% and 90%, respectively. From these data, several of the linear elastic material properties and uniaxial "yield strengths" were obtained. Also, the isotropic hardening curves at each moisture level were obtained from the MD stress-strain curves. The measured parameters are tabulated in Figure 10. To complete the formulation, several educated guesses were made for the remaining material parameters. These best estimate values are tabulated in Figure 11.

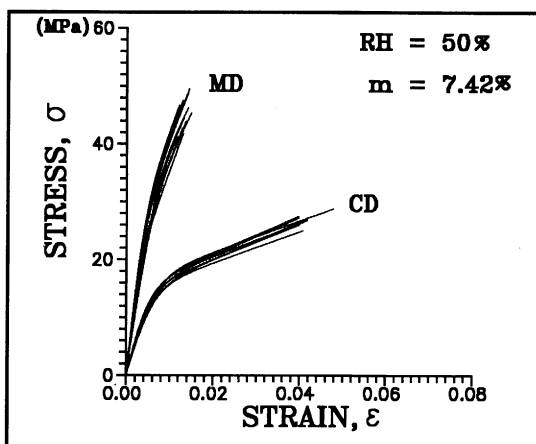


Figure 8 - Uniaxial Stress-Strain Curves for Paper

It is realized that the utilized inelastic constitutive model for the stress-strain behavior of the paper sheet is at best approximate. However, it has served as a test case on which to evaluate the effectiveness of the iterative nonlinear finite element technique for modeling the embossing

process. In ongoing work, emphasis is being placed on further refinement of the paper constitutive and failure formulations used within the ABAQUS modeling procedure.

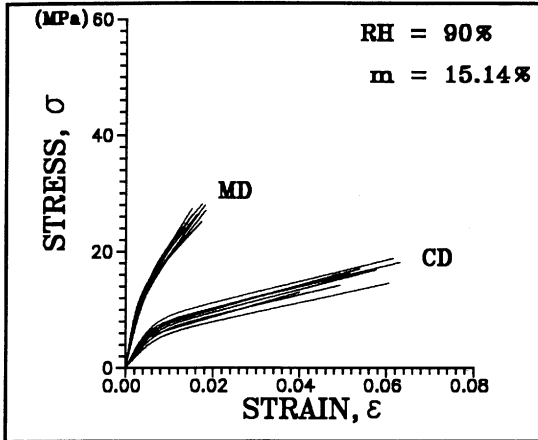


Figure 9 - Uniaxial Stress-Strain Curves for Paper

---

RH = 50%

$E_{11} = 6660.4$  MPa

$X = 6.66$  MPa

$E_{22} = 2739.1$  MPa

$Y = 4.66$  MPa

$\nu_{12} = 0.39$

$G_{12} = 1734.0$  MPa

RH = 90%

$E_{11} = 3972.7$  MPa

$X = 2.98$  MPa

$E_{22} = 1258.9$  MPa

$Y = 2.09$  MPa

$\nu_{12} = 0.40$

$G_{12} = 671.0$  MPa

---

Figure 10 - Measured Material Parameters

---

<u>RH = 50%</u>	
$E_{33} = 6660.4 \text{ MPa}$	$Z = 10 \text{ MPa}$
$\nu_{13} = 0.30$	$Q = 3.85 \text{ MPa}$
$\nu_{23} = 0.10$	$R = 3.46 \text{ MPa}$
$G_{13} = 1734.0 \text{ MPa}$	$S = 3.85 \text{ MPa}$
$G_{23} = 1734.0 \text{ MPa}$	
<u>RH = 90%</u>	
$E_{33} = 4500.0 \text{ MPa}$	$Z = 4.47 \text{ MPa}$
$\nu_{13} = 0.30$	$Q = 1.72 \text{ MPa}$
$\nu_{23} = 0.10$	$R = 1.55 \text{ MPa}$
$G_{13} = 671.0 \text{ MPa}$	$S = 1.72 \text{ MPa}$
$G_{23} = 671.0 \text{ MPa}$	

---

Figure 11 - Estimated Material Parameters

## RESULTS AND DISCUSSION

The finite element meshes in Figures 5 and 6 were analyzed for the cases of plane stress and plane strain using the loading and boundary conditions discussed earlier. For each embossing element, the maximum penetration was chosen to be 1 mm, and the calculations were performed with paper material properties at relative humidity levels of 50% and 90%. Figures 12 and 13 show the predicted plane stress deformations at the point of maximum penetration at 50% and 90% RH for the rounded rectangular and rounded circular embossing elements, respectively. The analogous results for plane strain are shown in Figures 14-15. Figures 16-19 show the associated predicted deformations after the embossing element has been retracted and no longer contacts the paper sheet. The deformations in the paper sheet in these illustrations are permanent as a result of the inelastic stresses and strains experienced by the sheet during the penetration step. The embossing element and rubber layer returned to exactly the same shapes as before loading since these materials were modeled as either rigid or elastic.

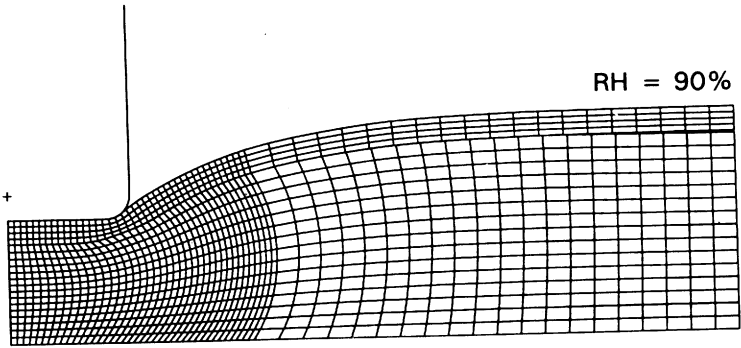
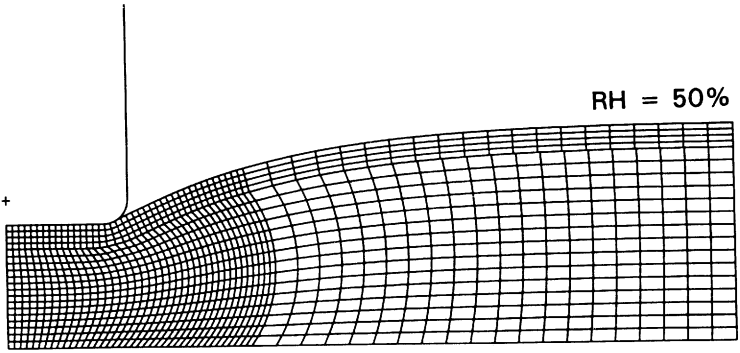
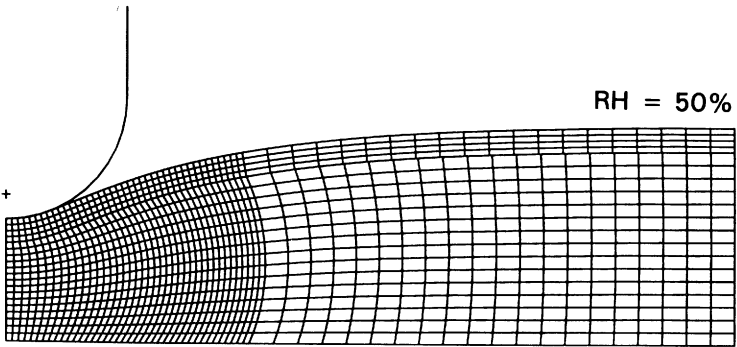


Figure 12 - Predicted Deformations at the Point of Maximum Penetration (Rounded Rectangular Element, Plane Stress)



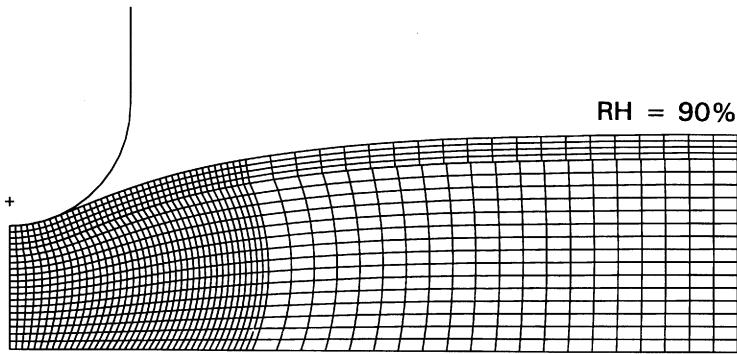


Figure 13 - Predicted Deformations at the Point of Maximum Penetration  
(Rounded Circular Element, Plane Stress)

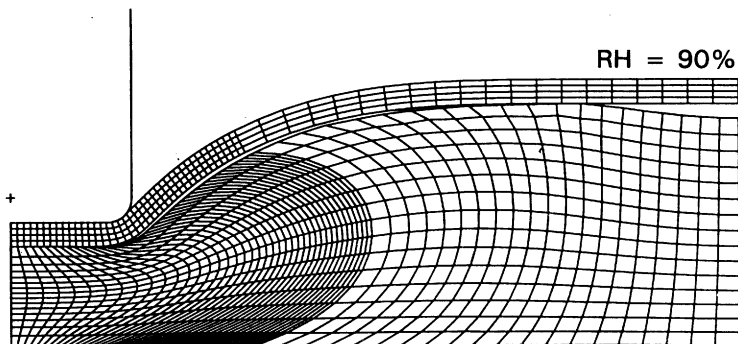
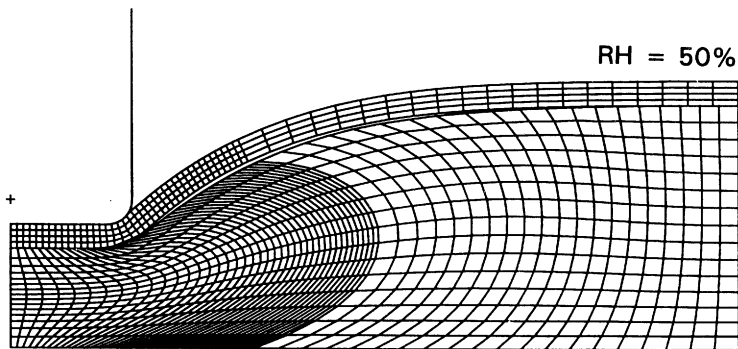


Figure 14 - Predicted Deformations at the Point of Maximum Penetration  
(Rounded Rectangular Element, Plane Strain)

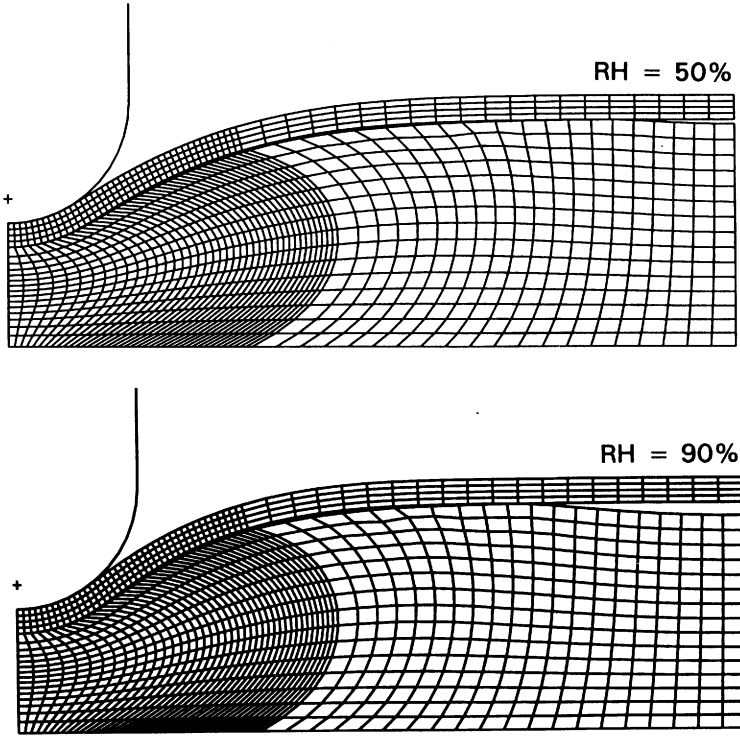


Figure 15 - Predicted Deformations at the Point of Maximum Penetration (Rounded Circular Element, Plane Strain)

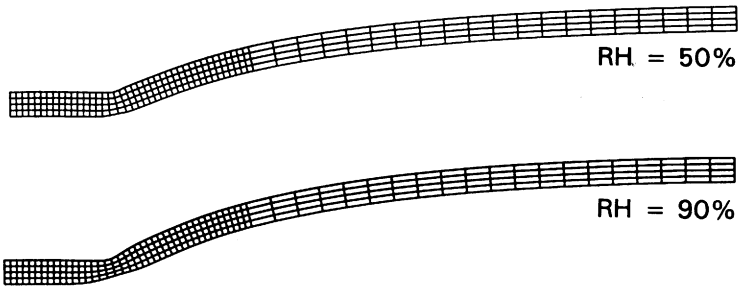
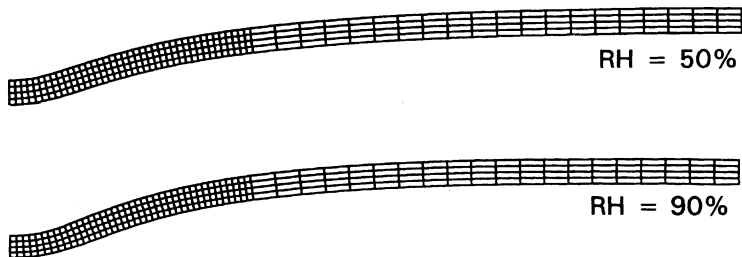
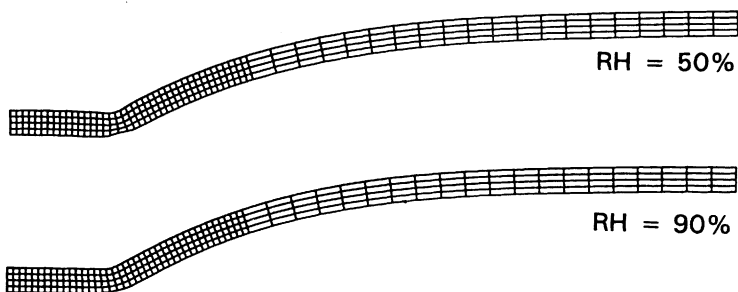


Figure 16 - Predicted Permanent Deformations (Rounded Rectangular Element, Plane Stress)



**Figure 17 - Predicted Permanent Deformations  
(Rounded Circular Element, Plane Stress)**



**Figure 18 - Predicted Permanent Deformations  
(Rounded Rectangular Element, Plane Strain)**

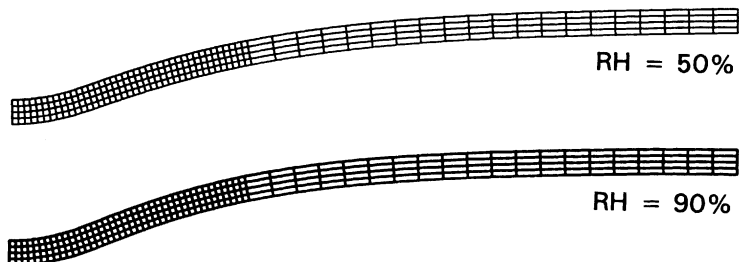


**Figure 19 - Predicted Permanent Deformations  
(Rounded Circular Element, Plane Strain)**

It is noted that the calculated permanent deformations differed significantly for the two different embossing elements. For a given embossing element, the differences in the permanent deformations for the plane stress and plane strain were less obvious. The permanent deformations for plane strain were slightly larger than the corresponding deformations for plane stress. This is due to the extra constraint of no out-of-plane (with respect to the finite element mesh) deformation present in the plane strain case. This causes larger vertical deformations in the rubber and paper, leading to larger permanent deformations in the paper. In fact, the large expansion in the rubber actually caused the portions of the paper sheet away from the embossing element to move upward relative to their original location prior to embossing. For the true case of a three-dimensional embossing element, the permanent deformations will lie between the plane stress and plane strain results.

Crimping occurred in the region of the paper which contacted the corner of the rounded rectangular embossing element. Also, the thickness of the sheet became noticeably more thin in that region after embossing. The rounded circular element created a much smoother permanent deformed shape for the paper sheet. As expected, it was found that the paper sheets were more easily formed at the higher moisture content where their stiffnesses and strengths were greatly reduced.

In addition to deformations, the finite element analyses calculated the stresses experienced in the paper sheet during the embossing process. For example, Figure 20 shows contour maps of the horizontal normal stress  $\sigma_x$  in the paper (RH = 50%) predicted at the positions of maximum embossing element penetration and after element retraction for the rounded rectangular element (plane stress). Figure 21 illustrates the corresponding plots for the paper sheet embossed by the rounded circular element. It is interesting to note that for both elements, the stresses at many points change signs between the two configurations. This is due to the plastic strains in the sheet which prevent it from returning to its original flat configuration. A similar behavior is seen in metallic beams in bending which are plastically deformed (22).

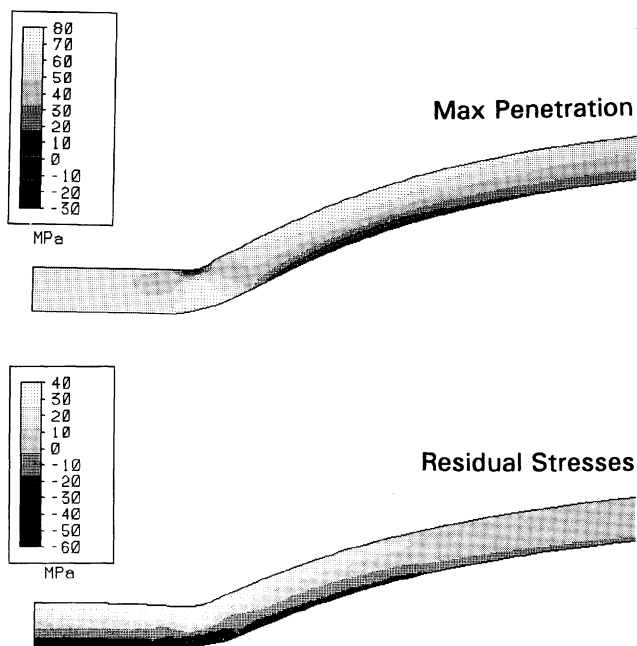
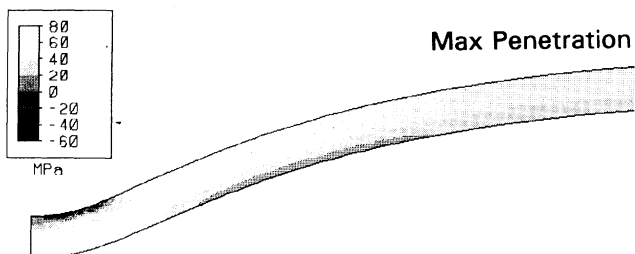
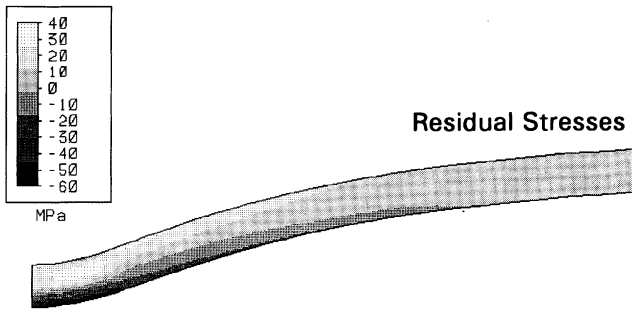


Figure 20 - Predicted Horizontal Normal stress  $\sigma_x$  Contours in the Paper (RH = 50%, Rounded Rectangular Element, Plane Stress)





**Figure 21 - Predicted Horizontal Normal stress  $\sigma_x$  Contours in the Paper (RH = 50%, Rounded Circular Element, Plane Stress)**

It is expected that both the permanent deformations and residual stress distributions have an important influence on the increased flexibility and compressibility of embossed papers. The changes in the stress-strain behavior and material properties of the paper sheets due to embossing have been predicted by calculating the uniaxial tension response of the embossed sheets. The embossing element, rubber layer, and all the interface elements were first removed from the finite element model. The permanently deformed sheets were then subjected to prescribed axial deformations in the x-direction (MD), and the axial loads at the boundary were calculated. Both plane stress and plane strain conditions for the uniaxial tensile specimen geometries were considered. The predicted axial load versus deformation data were transformed to stress-strain data using the original cross-sectional area and length of the paper sheet. For the plane stress case, Figure 22 shows the deformed shapes of the paper sheet embossed by the rounded rectangular element (RH = 50%) at various stages of the uniaxial tension analysis. Figure 23 illustrates corresponding plane stress plots for the paper sheet embossed by the rounded circular element. Similar results to those illustrated in Figures 22-23 have also been obtained for the plane strain case. It is noted that the sheets are returned to nearly flat configurations during the uniaxial tension loading process.

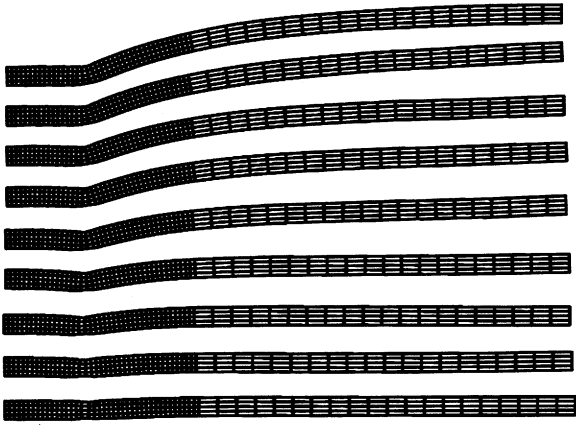


Figure 22 - Deformed Shapes for Uniaxial Tension of the Embossed Sheet (Rounded Rectangular Element, Plane Stress,  $RH = 50\%$ )

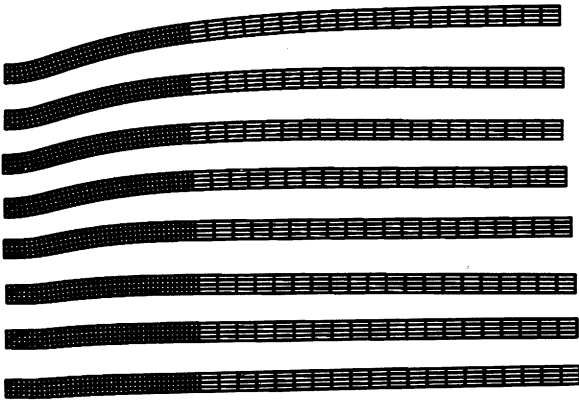


Figure 23 - Deformed Shapes for Uniaxial Tension of the Embossed Sheet (Rounded Circular Element, Plane Stress,  $RH = 50\%$ )

The stress-strain curves for the embossed sheets have been compared to those for the non-embossed paper. The results for both types of elements (plane stress and plane strain) are shown in Figures 24-25 for relative humidities of 50% and 90%, respectively. As expected, the paper sheets had significantly reduced stiffnesses after embossing, especially when the loadings were small. This is due to the permanent deformations in the embossed sheets which are removed during the uniaxial loading. As the curvature of the embossed sheets was reduced and they became flat, the stress-strain curves approached those of the non-embossed sheet. It was also noticed that the sheets embossed by the rounded circular embossing element exhibited slightly stiffer mechanical response than those embossed by the rounded rectangular embossing element.

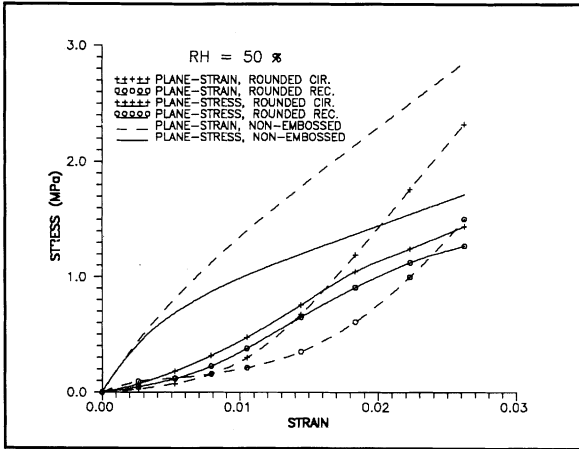


Figure 24 - Stress-Strain Curves for the Embossed Sheets at RH = 50%

**SUMMARY AND CONCLUSIONS**

A study on the paper embossing process has been performed using two-dimensional plane stress and plane strain finite element analyses. The iterative nonlinear finite element models incorporated nonlinear material behavior and plasticity, large deformations, and contact stresses. The residual stresses and permanent deformations in the embossed paper

sheets were calculated. Also, the changes in the mechanical behavior of the paper after embossing were predicted. The analyses showed that the shape of the embossing element and the moisture content of the paper play a very important role in the embossing process. Although the considered two-dimensional cases do not represent the true geometry exactly, they have served as test vehicles on which the performance of the iterative nonlinear finite element models can be evaluated. The execution times for the two-dimensional calculations are several orders of magnitude less than the corresponding three-dimensional calculations. Further experimental and analytical work is needed to improve the models used for the paper constitutive behavior.

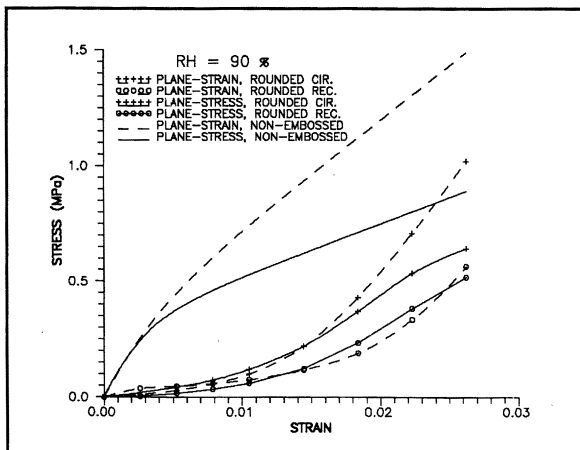


Figure 25 - Stress-Strain Curves for the Embossed Sheets at RH = 90%

## ACKNOWLEDGEMENTS

This research has been supported by the United States paper industry and the Auburn University Pulp and Paper Research and Education Center.

## REFERENCES

1. Lubkin, J. L., "Contact Problems," in Handbook of Engineering Mechanics, Edited by W. Flugge, McGraw-Hill, 1962, Chapter 42, pp. 1-12.
2. Kikuchi, N., "Seepage Flow Problems Using Variational Inequalities," International Journal of Numerical and Analytical Methods in Geomechanics, Vol. 1, 1977, pp. 283-297.
3. Kikuchi, N. and Oden, J. T., "Contact Problems in Elasticity," Texas Institute of Computational Mechanics (TICOM) Report 79-8, University of Texas, 1979.
4. Kikuchi, N. and Oden, J. T., Contact Problems in Elasticity: A Study of Variational Inequalities and Finite Element Methods, Society for Industrial and Applied Mathematics (SIAM), 1988.
5. Holzner, M. and Mannl, V., "Mechanics of Drawing with Rubber Pads," Proceedings of the Second International Conference on Technology of Plasticity, Edited by K. Lange, Stuttgart, Germany, August 24-28, 1987, pp. 1151-1157.
6. Sih, G. C., Chao, C. K., Lui, C. H. and Lin S. Y., "Deep Drawing of Plastically and Incrementally Deformed Circular Cylindrical Cup," Theoretical and Applied Fracture Mechanics, Vol. 15(1), 1991, pp. 35-62.
7. Saran, M. J., Pifko, A. B., Kikuchi, N. and Tamma, K. K., Numerical Methods for Simulation of Industrial Metal Forming Processes, AMD-Vol. 156, American Society of Mechanical Engineers, 1992.
8. ABAQUS User's Manual, Version 4-8, Hibbitt, Karlsson, and Sorensen, Incorporated.
9. Green, A. E. and Zerna, W., Theoretical Elasticity, Second Edition, Oxford University Press, 1968.

10. Malvern, L. E., Introduction to the Mechanics of a Continuous Medium, Prentice-Hall, 1969.
11. Perkins, R. W., "Models for Describing the Elastic, Viscoelastic, and Inelastic Mechanical Behavior of Paper and Board," in Handbook of Physical and Mechanical Testing of Paper and Paperboard, Edited by R. E. Mark, Marcel Dekker, 1983, pp. 23-75.
12. Suhling J. C., "Continuum Models for the Mechanical Response of Paper and Paper Composites: Past, Present, and Future," in Material Interactions Relevant to the Pulp, Paper, and Wood Industries, MRS Vol. 197, Edited by D. F. Caulfield, J. D. Passaretti, and S. F. Sobczynski, Materials Research Society, 1990, pp. 245-255.
13. Thorpe, J. L., "Paper as an Orthotropic Thin Plate," TAPPI, Vol. 64(3), 1981, pp. 119-121.
14. Suhling, J. C., Johnson, M. W., Rowlands, R. E. and Gunderson, D. E., "Nonlinear Elastic Constitutive Relations for Cellulosic Materials," in Mechanics of Cellulosic and Polymeric Materials, Edited by R. W. Perkins, ASME, AMD-Vol. 99, 1989, pp. 1-13.
15. Paetow, R. and Gottsching, L., "The Two-Dimensional Nonlinear Elastic Material Law for Paper," Presented at the 1990 Progress in Paper Physics Seminar, Kalamazoo, MI, September 30 - October 3, 1990.
16. Ramasubramanian, M. K. and Ko, Y. C., "Relationship Between the In-Plane Paper Properties and the Ball Burst Strength," in Mechanics of Cellulosic and Polymeric Materials, Edited by R. W. Perkins, ASME, AMD-Vol. 99, 1989, pp. 105-111.

17. Perkins, R. W., Sinha, S. and Mark, R. E., "Micromechanics and Continuum Models for Paper Materials of Medium to High Density," in Proceedings of the 1991 International Paper Physics Conference, Kona, Hawaii, September 22-26, 1991, pp. 413-435.
18. Tate, A., "A New Approach to the Theory of Plastic Deformation," International Journal of Solids and Structures, Vol. 14, 1978, pp. 475-497.
19. Hill, R., Mathematical Theory of Plasticity, Oxford University Press, 1950.
20. Rowlands, R. E., "Strength (Failure) Theories and Their Experimental Correlation," in Handbook of Composites, Vol. 3, Edited by G. C. Sih and A. M. Skudra, Elsevier, 1985, pp. 71-125.
21. Yeh, K. C., Considine, J. M. and Suhling, J. C., "The Influence of Moisture Content on the Nonlinear Constitutive Behavior of Cellulosic Materials," in Proceedings of the 1991 International Paper Physics Conference, Kona, Hawaii, September 22-26, 1991, pp. 695-711.
22. Kachanov, L. M., Fundamentals of the Theory of Plasticity, Mir Publishers, 1974.

## **Transcription of Discussion**

### **FINITE ELEMENT MODELLING OF THE EMBOSSING OF TOWEL AND TISSUE**

J C Suhling, S Liang

#### **Dr J E Luce, International Paper Co, USA**

Your explanation of the residual compression forces at the bottom of the embossings might well be true, However, we have attributed the microcompressions and macrocompressions in the fibres in that area to an effect very much like 'Clupacking' caused by the resilient rubber backing compressing the paper in-plane. This is borne out to some extent by the fact that we have not seen these microcompressions when we use matched metal-to-metal embossing rolls.

#### **J Suhling**

I think you're observation is correct and maybe a combination of those two factors at once. The rubber doesn't really allow the paper to go anywhere and equally the embossing element on the other side doesn't allow the paper to do much either so you have a lot of constraints there until everything is released and the residual compressive force effect would only happen after all these things are separated.

#### **J F Waterhouse, IPST, USA**

There are obviously board moulding processes where your work would be important so I shouldn't be embarrassed about having to present results for board instead of tissue. I certainly agree with your analysis about the residual stress distribution as obviously there has to be a change in residual stress to maintain the shape that you have after embossing. I was wondering what effect

accounting for the initial residual stress distribution might have in your analysis.

**J Suhling**

No consideration of the initial internal stresses has been made.

**J Waterhouse**

One of the useful things in moulding is being able to determine the spring back and I presume you can determine that from your analysis.

**J Suhling**

Yes we can. In our analysis we basically kept the sheet in a sense tensioned when we released. We could indeed take off those boundary conditions on the release step where the embossing element is raised.

**Dr T Uesaka, Pulp and Paper Research Institute of Canada**

It is very interesting work. You mentioned the kink formation in one of the graphs. Does this happen within the paper structure or are you talking about the whole shape of paper?

**J Suhling**

The kink was in the corner, I mean it was a visible kink but as to the local effects of that I cannot say.

**T Uesaka**

So you are not talking about the local deformation as a kink.

**J Suhling**

I just noticed a macro kink in that area. That is what I was referring to.

**T Uesaka**

Normally this kink is sensitive to the selection of the yield surface. Depending on the shape of the yield surface if you have a slightly rough surface you can see some kink formation. That is local buckling phenomena. However you used very smooth yield surfaces.

**J Suhling**

Yes our yield surface was smooth.

**T Uesaka**

From a numerical point of view it is a very interesting result.

**Prof J Lindsay, IPST, USA**

Have you considered applying this to multiply structures where you would have different physical properties in 2 or 3 layers.

**J Suhling**

We've considered two layers of that material that we cannot talk about. (Tissue)

**J Lindsay**

Have you also considered applying your model to the scoring of board?

## **J Suhling**

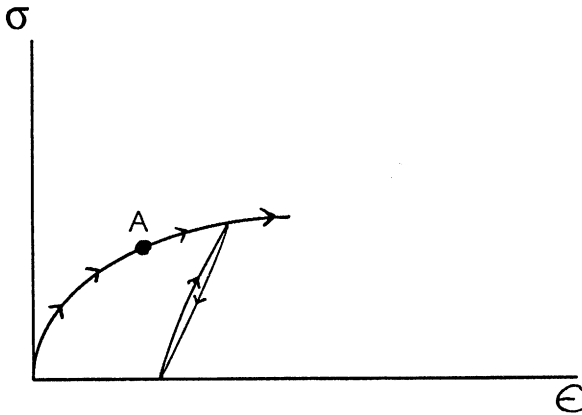
We have not considered that but these are the type of analyses which would need to be performed to get an accurate prediction of what would happens in scoring. You need the same type of numerical intensity that one needs to model all the non-linearities that are involved here.

## **Dr R Popil, MacMillan Bloedel, Canada**

The stress/strain relationships that you use are essentially Hooke's law and therefore you have a linearity between the stress and the strain but no retardation/relaxation terms describing the viscoelastic nature of the whole problem. How does that effect the dynamics of your embossing process in other words, the speed of the whole process should affect your final result and secondly, how do the stress/strain relationships used lead to a permanent strain after the embossing process?

## **J Suhling**

As far as the speed goes the models didn't consider that the stress/strain curve is different for different speed rates. The embossing process generally is quite fast in production so we would want to use a stress/strain curve measurement under near ultrasonic conditions or measured very quickly with a mechanical tester. As to how the actual embossing became permanent deformation from the stress/strain behaviour. We used the linear part of the stress/strain curve prior to inelastic deformations, and then a plasticity model as shown.



At anything beyond point A or wherever we defined as the top of the linear region, would give you some permanent strains after unloading. That's how the permanent deformations came in.

**R Popil**

I would suggest that perhaps the model could be a little more elaborate if viscoelastic terms were to be incorporated into the work.

**J Suhling**

I agree with you completely. The model, aside from being more elaborate, might also be impossible.

**R Popil**

That's beside the point!

**J Suhling**

I am anxious to work on this problem beyond the next century if possible.

**P McKinley, AMCOR, Australia**

Did you run into the situation where you had to worry about element distortion and the possibility of remeshing?

**J Suhling**

We ran into situations where we had trouble in getting convergence and maybe that would have been an option. We have switched to the explicit formulation of the code now which includes time dependence but is seemingly able to handle more easily the great non-linearities and large deformations. These were implicit calculations and I think that if you understand what these mean (the audience that is) this affects the convergence of the model and we are anxious to get our models to converge more easily and get our results faster in the future. But we have not remeshed at this time.

**B Phillips, Shotton Paper Co, UK**

Would you like to think about some other applications of the finite element method perhaps related to the winding of a newsprint reel, how about modelling the nip force between the wind up reel and the solid roll. We might find it quite interesting to see what's going on in that situation.

**J Suhling**

I agree with you completely. I think that there are several of us who would love to apply the finite element analysis to other situations in the paper industry. It's a matter of time and money.

**Prof H Kropholler, UMIST, UK** (additional contribution added after the Symposium)

In the paper presented by J C Suhling and S Liang 'Finite element modelling of paper products' the deformation of the paper or board during the embossing operation is described. Here a technique for evaluating the quality of an essentially linear pattern using the 2D-fft is given. The specific example relates to the quality, coarseness or fineness, of creping of tissue. The equipment shown in figure 1 is again used. However, the image is obtained by reflection, with the flash placed at an angle of about  $45^\circ$ . Two examples of creping are shown in figure 6 in which it is clear that the creping is coarser in one of the examples. The quality of the crepe is dependant on the state and angle of attack of the blades. Once again the 2D-fft can be used. As shown in figure 7 the area of interest is contained in an angle. Schematically this is the cross-hatched area of figure 8. A plot of the energy or power is shown in figure 9 where the differences between the two samples is clearly quantified.

These two examples illustrate a novel way in which the two-dimensional fourier transform power spectrum can be used to assess non-periodic characteristics of paper and that data can be obtained on-line.

The studies presented in this contribution were carried out by A R Guesalaga of the Department of Electrical Engineering, Catholic University of Chile, Santiago, Chile and X A Fernando, CMPC, Santiago, Chile.

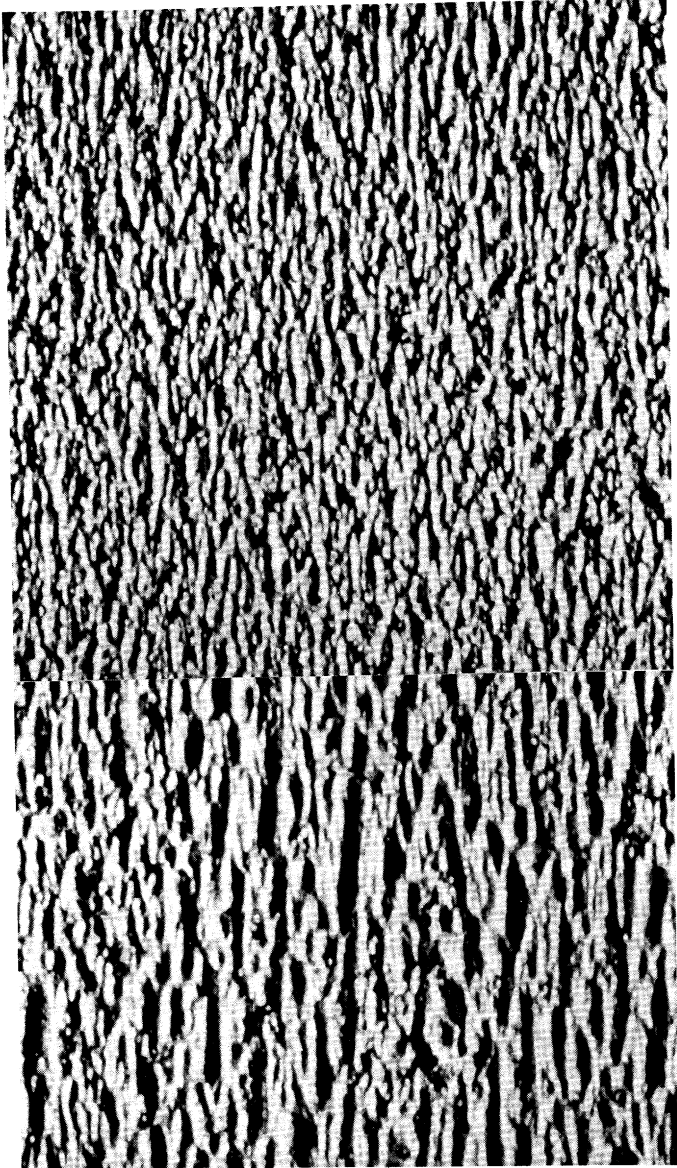


**Figure 6** Coarse versus fine creping

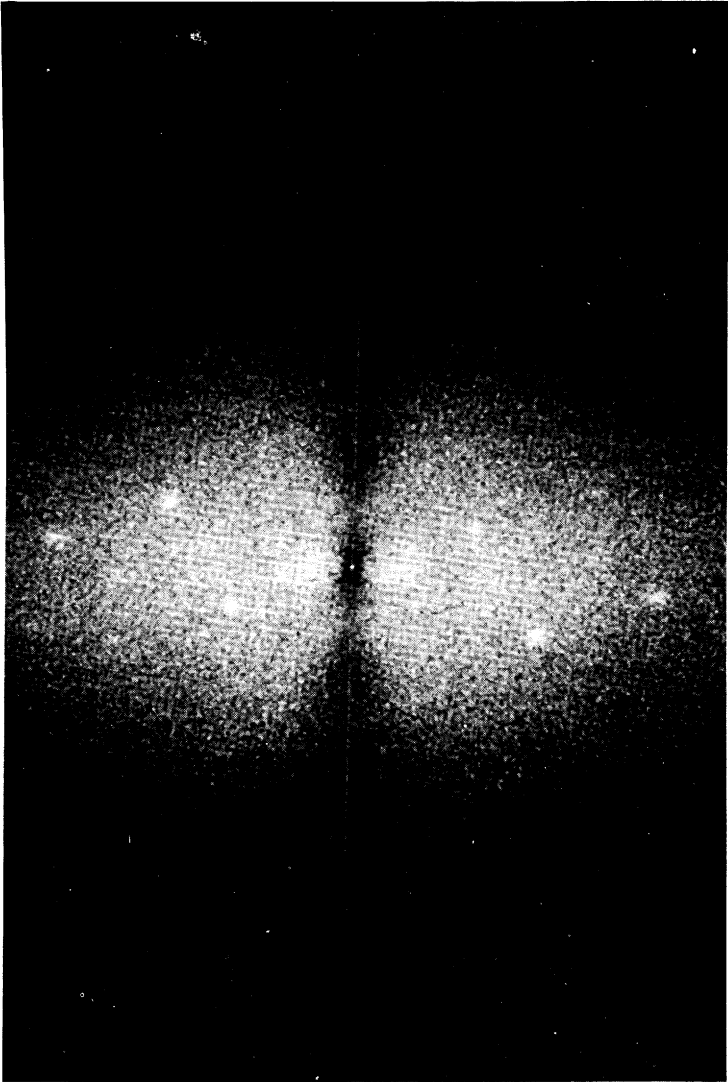


**Figure 7** Power spectrum for creped tissue

# Two-dimensional Spectrum

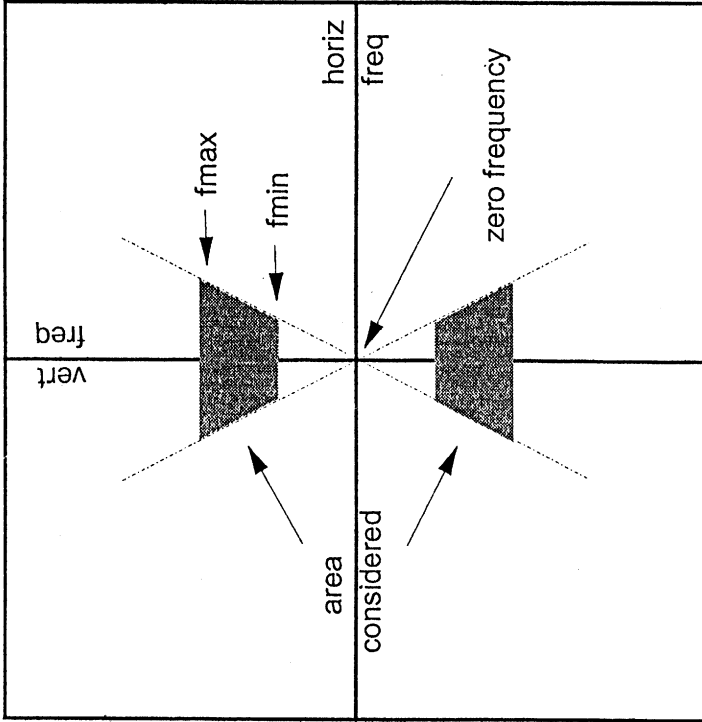


Figure 8 Method of creeping measurement

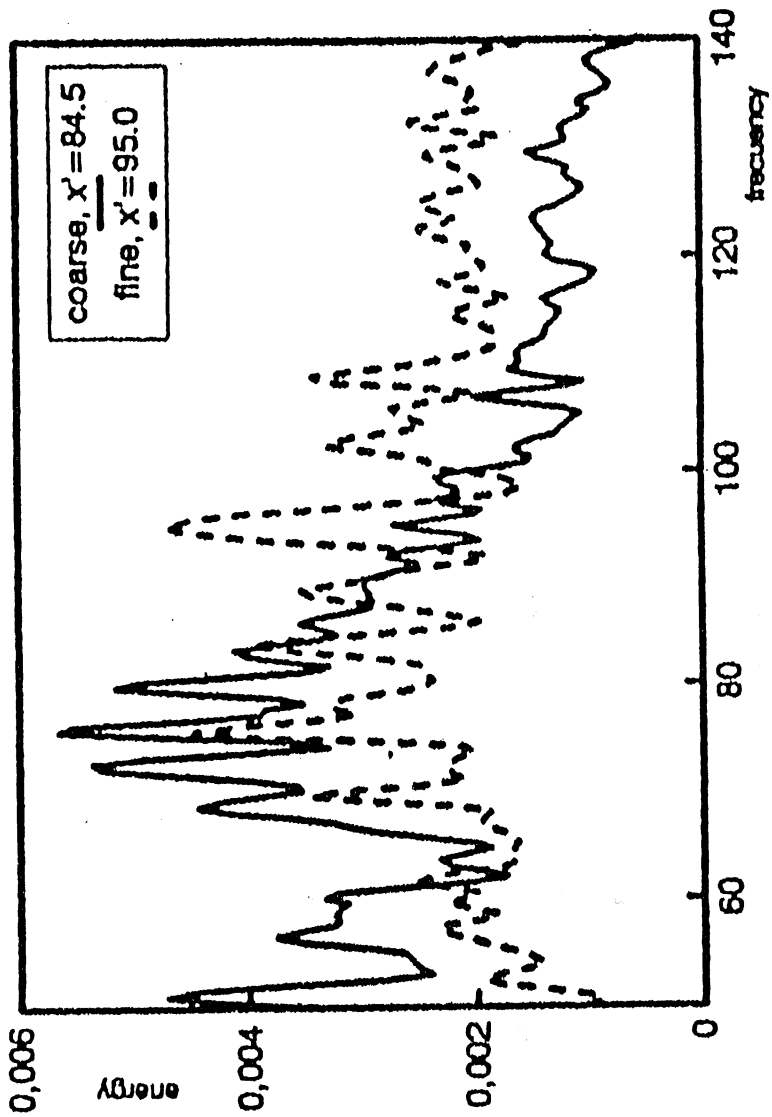


Figure 9 Energy distribution of creeping spectrum